Investigation of predominant area of the directivity effect for strong ground motions near faults

K. Miyakoshi &Y. Nishimura
Geo-Reserch Institute, Japan

T. Sasatani
Former Hokkaido Univ., Japan

K. Kamae
Research Reactor Institute, Kyoto Univ., Japan

K. Irikura
Aichi Institute of Technology, Japan

SUMMARY:
In this study we investigate the near-fault rupture directivity effect (NFRD effect) in strong ground motion during the 2004 Rumoi earthquake (*M*j 6.1) using Hybrid simulation, which uses a combination of 3D-FDM (3D Finite Difference Method) and SGF (Stochastic Green's Function). We calculated seismograms near the fault area (20 km x 20 km) and made a PGV distribution map. Strong ground motions over 70cm/s, which are affected by the NFRD effect, appeared around the surface projection line of the upper edge of the rupture area. We extracted the predominant area of the NFRD effect on near-source strong ground motions using the criteria of Ohno et al. (1998). Additionally we attempted to select a large PGV zone in the predominant area of the NFRD effect using a PGV attenuation curve (Si and Midorikawa, 1999). As a result, we successfully selected a large PGV zone affected by the NFRD effect near the fault area.

Keywords: 2004 Rumoi earthquake, strong ground motions, Hybrid simulation, NFRD effect

1. INTRODUCTION

Rupture directivity effects cause spatial variations in strong ground motion amplitude near the fault. An inland crustal earthquake (*M*j 6.1) occurred on December 14, 2004 in the northern part of Hokkaido, Japan (2004 Rumoi earthquake). The source mechanism is reverse fault with low dip angle (25 degrees). Strong ground motions over 1,000 cm/s^2 and 70 cm/s were recorded at the nearest strong-motion station (HKD020) about 10 km from the hypocenter as shown in Fig.1. Table 1 shows the source parameters of the 2004 Rumoi earthquake. Using the EGF (Empirical Green's Function) method, Maeda and Sasatani (2009) concluded that the large strong ground motions at HDK020 are mainly affected by the source effects (forward directivity and shallow position of asperities). Miyakoshi et al. (2009) also validated these source effects with simulation using the discrete wavenumber method (Bouchon, 1981) together with the reflection transmission matrix method (Kennett and Kerry, 1979) in laterally homogeneous (1D) velocity structure.

It is important to investigate the predominant area of the near-fault rupture directivity (NFRD) effect (Somerville et al., 1997) for the strong ground motions around HKD020. Consequently, we calculated seismograms near the fault area and made a PGV (Peak Ground Velocity) distribution map (20 km x 20 km). We used Hybrid simulation, which uses a combination of 3D-FDM (3D Finite Difference Method) and SGF (Stochastic Green's Function). We attempted to extract the predominant area of the NFRD effect on near-source strong ground motions.

2. HYBRID SIMULATION

We used 3D-FDM based on Pitarka (1999) for the long period range and the SGF method (Kagawa, 2004) based on Boore (1991) for the short period range. As there is no existing 3D velocity structure

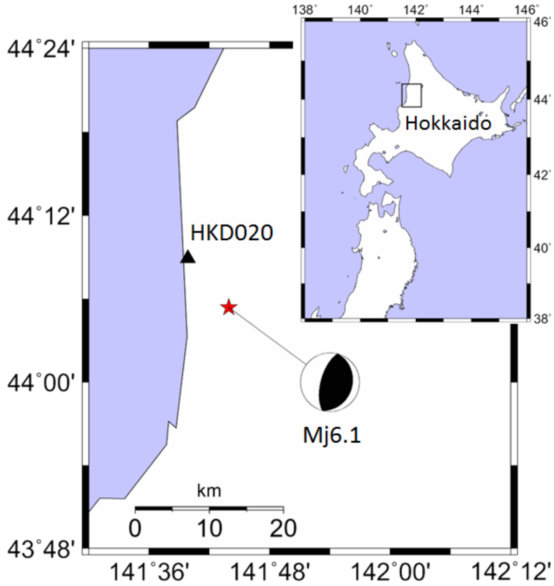

Figure 1. Location of the 2004 Rumoi earthquake. Star denotes epicenter and triangle denotes strong-motion station (HKD020). The study area is also indicated by the rectangle in the insert.

Table 1 Source parameters of the 2004 Rumoi earthquake (Maeda and Sasatani, 2009)

Date	2004/12/14, 14:56(JST)
Epicenter	44.0897N, 141.7322E
Depth (km)	5.3
Strike(degree)	N15E
Dip (degree)	25
Mj	6.1
Mo (Nm)	4.44 x 10^{17} (F-net)

model near HKD020, a laterally homogeneous velocity structure at HKD020 (Maeda and Sasatani, 2009) is assumed for 3D-FDM simulation. The subsurface structure model is shown in Table 2. The simulation area for 3D-FDM is 20 km x 20 km, divided by a 0.025 km grid, for the period range longer than 0.2 sec. About 640,000 points are simulated in total. We also performed SGF simulation at each 0.250 km grid point in the same area. Finally we made a PGV distribution obtained from the Hybrid simulation at each 0.250 km grid. To simplify the calculation of 3D-FDM, we replaced the first 3 layers (Layers 1 - 3) by Layer 4 in Table 2. Meanwhile, we used all layers (Layers 1 - 7) in Table 2 for SGF calculations. Table 3 shows the source parameters in the strong motion generation area (SMGA). We assumed short and long period strong ground motions generated in the SMGA. We did not assume a rupture area for the Hybrid simulation in this study. The transition period range between 3D-FDM and SGF was estimated to be from 0.16 to 0.25 sec (from 4 to 6 Hz) by trial and error, comparing the simulation result and observed data at HKD020. Fig. 2 shows the Hybrid simulation result (red solid line) in comparison with observed data (black solid line) at HKD020. The simulation has good agreement with observations. In view of this result, the source model and velocity structure model used in this study were considered adequate for the Hybrid simulation.

The PGV distribution map (20 km x 20 km) near the fault area is shown in Fig. 3. The triangle marks HKD020 and the star marks the rupture starting point. The outer and inner black broken line rectangles delineate the ‘imaginary’ rupture area and SMGA, respectively. The black solid line is the surface projection line based on the dipping angle (25 degrees) of the ‘imaginary’ rupture area. The red broken line rectangle delineates the predominant area of NFRD effect (Ohno et al., 1998). In a later section we explain how to determine the ‘imaginary’ rupture area and the predominant area of NFRD effect. From Fig. 3, it is clear that large strong ground motions over 70 cm/s appear about 4 km east from HKD020. Large strong ground motions are affected by the NFRD effect. Fig.4 shows examples of pseudo velocity response spectra (pSv) for EW components at each grid point in the simulation area. We also plotted pSv (orange line) of the blind fault in the upper crust (Kato et al., 2004, hereafter Kato's spectrum). They showed the upper level of seismic ground motions caused by blind faults on the basis of near-source strong motion records observed on rock sites in Japan and California. A blind fault is defined by Kato et al. (2004) as a fault that cannot be identified in advance by detailed geological surveys. However, because of the nearby Rikibiru active fault, the 2004 Rumoi earthquake is not necessarily classified as a blind fault. Averaged pSv values within 15 km of the fault distance (Si and Midorikawa, 1999) are shown in Fig. 3 by the white solid line. White broken lines denote standard deviations. The averaged pSv and its +1 sigma are lower than Kato's spectrum. The averaged area within 15 km of the fault distance almost covers the simulation area (20 km x 20 km) as shown in Fig. 3. It is obvious that small PGV, which are not affected by NFRD effects, are mainly contained within 15 km of the fault distance. Consequently, we need to extract the predominant area of the NFRD effect on near-source strong ground motions.

Table 2 Laterally homogeneous subsurface structure model at HKD020

Layer No.	Vp km/s	Vs km/s	Density g/cm^3	Depth km
1	0.380	0.160	1.6	0.000
2	0.740	0.300	1.6	0.001
3	1.380	0.500	2.0	0.003
4	2.000	0.710	2.0	0.007
5	3.500	1.850	2.2	1.000
6	4.493	2.567	2.3	2.000
7	5.196	3.000	2.7	3.800

Table 3 Source parameters in Strong Motion Generation Area (SMGA)

Area (km^2)	4.41
Mo (Nm)	6.53×10^{16}
Stress drop (MPa)	17.2
Rise time (s)	0.4
Rupture velocity (km/s)	2.7
Rake angle (degree)	90

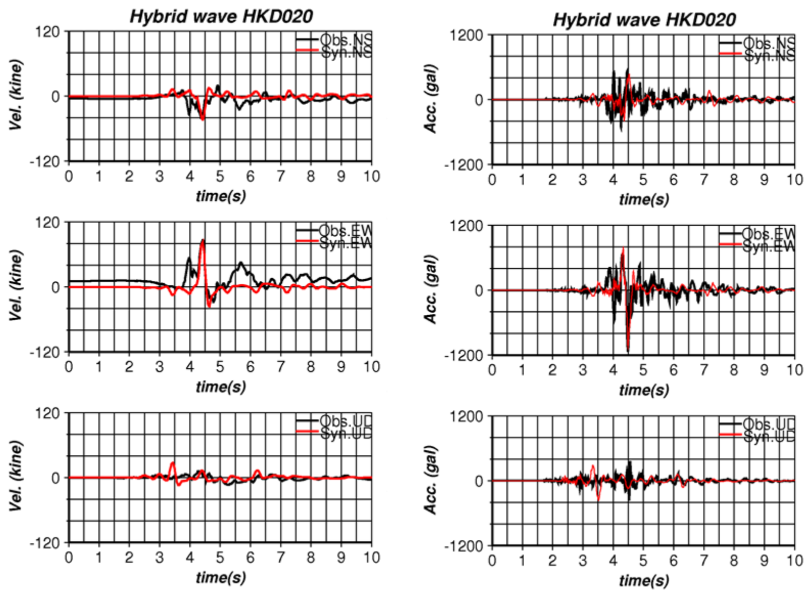

Figure 2. Hybrid simulations (red) comparing with observed data (black) at HKD020. Left panels show velocity and right panels show acceleration seismograms. The three traces from top to bottom show NS, EW and UD components, respectively.

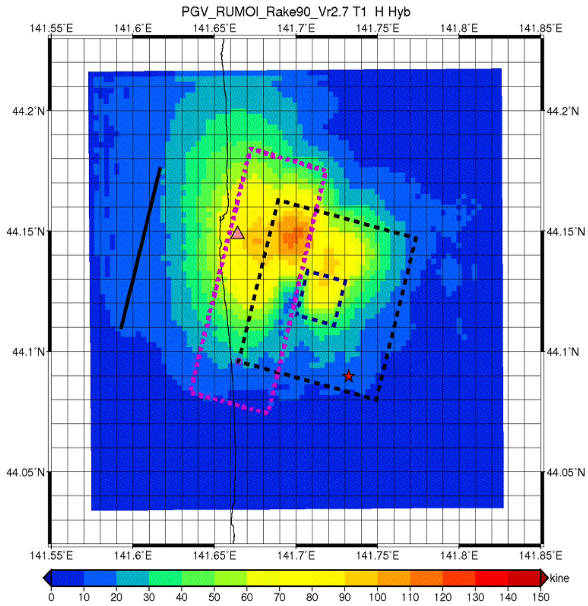

Figure 3. PGV distribution map (20 km x 20 km) obtained from the Hybrid simulation. Triangle marks HKD020, and star marks rupture starting point. Outer and inner black broken line rectangles delineate the 'imaginary' rupture area and SMGA, respectively. Black solid line is the surface projection line based on dipping angle (25 degrees) of the rupture area. Red broken line rectangle delineates the predominant area of NFRD effect.

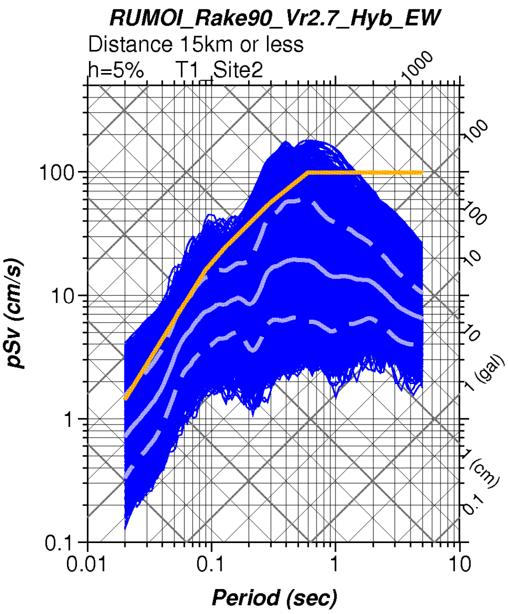

Figure 4. Examples of pseudo velocity response spectra (pSv) for EW components in simulation area (20 km x 20 km). White solid line denotes averaged pSv within 15 km of the fault distance (Si and Midorikawa, 1999). White broken lines denote standard deviations. The pSv (orange line) of the blind fault in the upper crust (Kato et al., 2004) is also shown in this figure.

3. PREDOMINAT AREA OF THE NFRD EFFECT

First we tried to extract the predominant area of the NFRD effect using criteria from Ohno et al. (1998). They defined the predominant area of the NFRD effect for the reverse fault type as an area having size ±0.25L and centered on the projection of the upper edge of rupture area, where L is the length of the surface projection line. However, the rupture area is not assumed in this study, so we needed to set an ‘imaginary’ rupture area for extraction of the predominant area of the NFRD effect. We set the ‘imaginary’ rupture area of the 2004 Rumoi earthquake with reference to Maeda and Sasatani (2009) as below.

Step1: Using empirical scaling relationship (Somerville et al, 1999), we estimated the size of the rupture area ($S = 60.24\ km^2$) from the moment ($Mo = 4.44x10^{17}$ Nm) of the 2004 Rumoi earthquake.

Step2: Assuming a square rupture area (L = W), we obtained the rupture area length (L = 7.76 km).

Step3: We assumed the depth (2.8 km) of the upper edge of rupture area with reference to aftershock distribution (Maeda and Sasatani, 2009).

Fig.5 shows the source model of the 2004 Rumoi earthquake. The yellow square marks the SMGA estimated by Miyakoshi et al. (2009) using simulation. The red square marks the ‘imaginary’ rupture area obtained from Steps 1 - 3. The open and gray rectangles are the assumed fault plane and estimated SMGAs obtained using the EGF method (Maeda and Sasatani, 2009), respectively. Their main SMGA is slightly larger than our SMGA (yellow square in Fig.5). They also assumed two SMGAs as shown in Fig.5. There is discrepancy between our estimated SMGA and their SMGAs concerning number of SMGA and size of SMGA. However, the large pulse of strong ground motion at HKD020 (see Fig. 2) is explained by the Hybrid simulation calculated from only one SMGA (yellow square in Fig.5). Small SMGA in Fig.5 is obviously needed to explain strong ground motions at other sites (Maeda and Sasatani, 2009). Finally, we obtained the predominant area of NFRD effect (blue broken line rectangle) as shown in Fig. 5. The red broken line rectangle in Fig. 3 is same as the predominant area of NFRD effect in Fig.5. It is recognized that the predominant area of NFRD effect still contained small PGV (< 30cm/s), which is not affected NFRD effect, in the southern zone as shown in Fig.3. Furthermore we need to precisely select the predominant area of NFRD effect.

Next we tried to detect the large PGV zone in the predominant area of NFRD effect using the PGV attenuation curve of Si and Midorikawa (1999). Fig.6 shows the PGV attenuation obtained from the Hybrid simulation. Red dots show the PGV in the predominant area of NFRD effect. The PGV attenuation curve is also shown in Fig. 6 by the green solid line. The green broken lines show standard deviation (± 1 sigma) and the blue chain line shows + 2 sigma. The slope of PGV distribution (fault distance > 4 km) is apparently steeper. This apparent steep slope of PGV is in large part due to the neglect of rupture area for the Hybrid simulation in this study. We selected the PGV greater than average PGV +1 sigma (green broken line). The shaded zone in Fig.7 shows the area that has PGV greater than average PGV +1 sigma. It is obvious that we could use the PGV attenuation curve to select the large PGV zone in the predominant area of NFRD effect. Fig.8 shows examples of pSv for EW components. Red solid lines show pSv within the shaded zone in Fig.7. White solid line denotes averaged pSv and white broken lines denote standard deviation (± 1 sigma). The averaged pSv is almost same as the Kato’s spectrum and its +1 sigma is higher than Kato’s spectrum.

4. SHIFT OF RUPTURE STARTING POINT

In the preceding section, the rupture starting point is outside the SMGA as shown in Fig. 7. According to the recipe for the prediction of strong ground motion (Headquarters for Earthquake Research Promotion, 2009), rupture starting point is often set on the edge of SMGA. So we investigate the availability of the predominant area of NFRD effect using the PGV attenuation curve for variation of rupture starting point. Fig.9 (a), (b), (c) show the difference of PGV distribution for variation of rupture starting points. Shaded zones in Fig.9 show the predominant area of NFRD effect using PGV attenuation curve. The shaded zones successfully contained the large PGV zone. Fig.10 (a), (b), (c) show pSv for variation of rupture starting point. The averaged pSv (white solid line) is almost same as the Kato’s spectrum and its +1 sigma (white broken line) is higher than Kato’s spectrum for variation of rupture starting point.

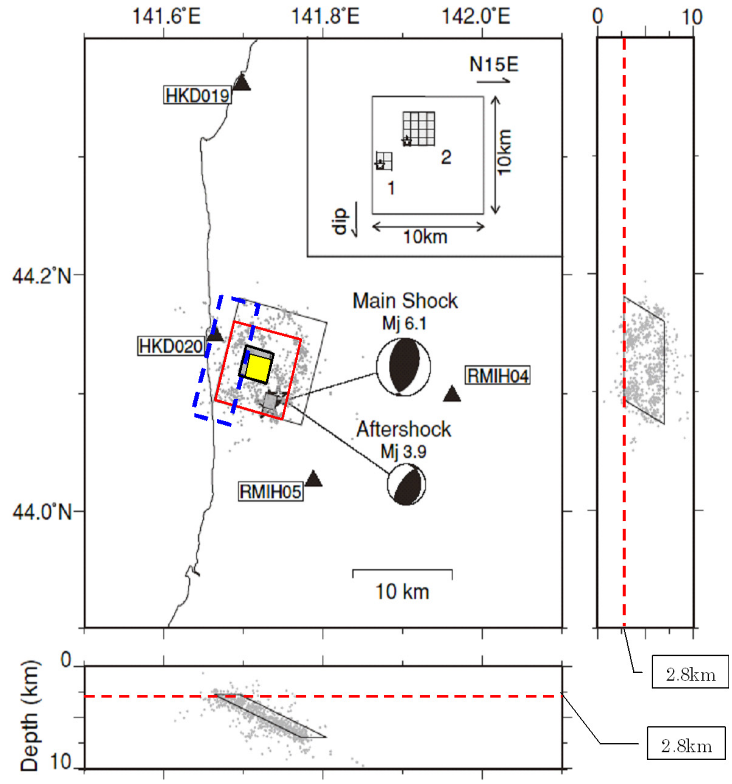

Figure 5. The source model of the 2004 Rumoi earthquake (adding figure from Maeda and Sasatani, 2009). Yellow rectangle is the SMGA estimated by Miyakoshi et al. (2009) using simulation. Red square marks the 'imaginary' rupture area. Blue broken line rectangle marks the predominant area of NFRD effect. Red broken line is the depth of upper edge of 'imaginary' rupture area. Dots show distribution of aftershocks. Open and gray rectangles are the assumed fault plane and estimated SMGAs using EGF method (Maeda and Sasatani, 2009), respectively. Triangles are strong motion observation sites.

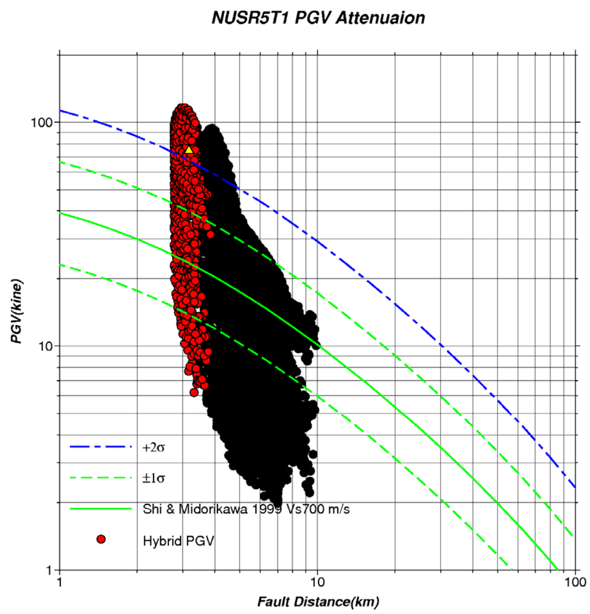

Figure 6. PGV attenuation obtained from the Hybrid simulation. Red dots show the PGV in the predominant area of NFRD effect. Black dots show PGV out of the predominant area of NFRD effect. Yellow triangle shows PGV at HKD020. The PGV attenuation curve (Si and Midorikawa, 1999) is also shown in this figure by green solid line. Green broken lines show standard deviation (± 1 sigma) and blue chain line shows + 2 sigma.

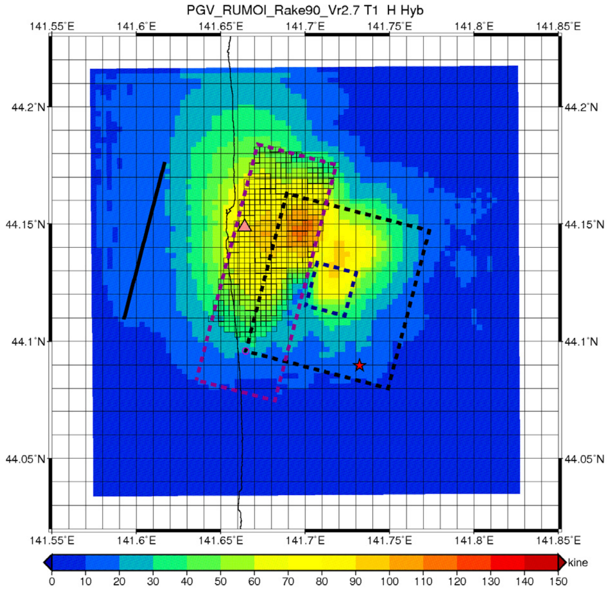

Figure 7. Predominant area of NFRD effect using PGV attenuation curve (shaded zone). Shaded zone indicates large PGV greater than average PGV +1 sigma in Fig. 6. Broken red line rectangle is the same as the predominant area of NFRD effect in Fig. 5.

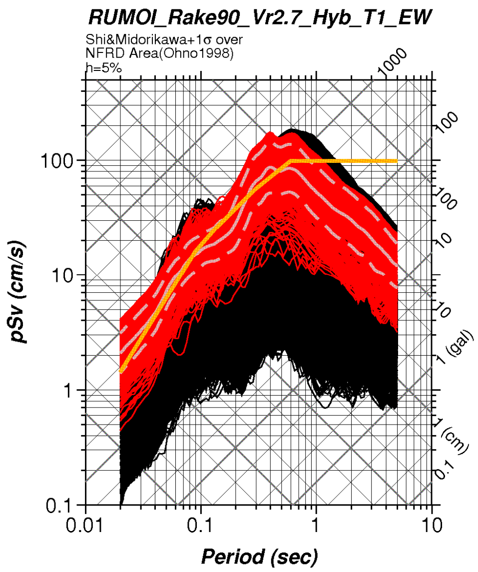

Figure 8. Examples of the pSv (red solid line) for EW components in shaded zone (the predominant area of NFRD effect using PGV attenuation curve) as shown in Fig.7. White solid line denotes averaged pSv. White broken lines denote standard deviations.

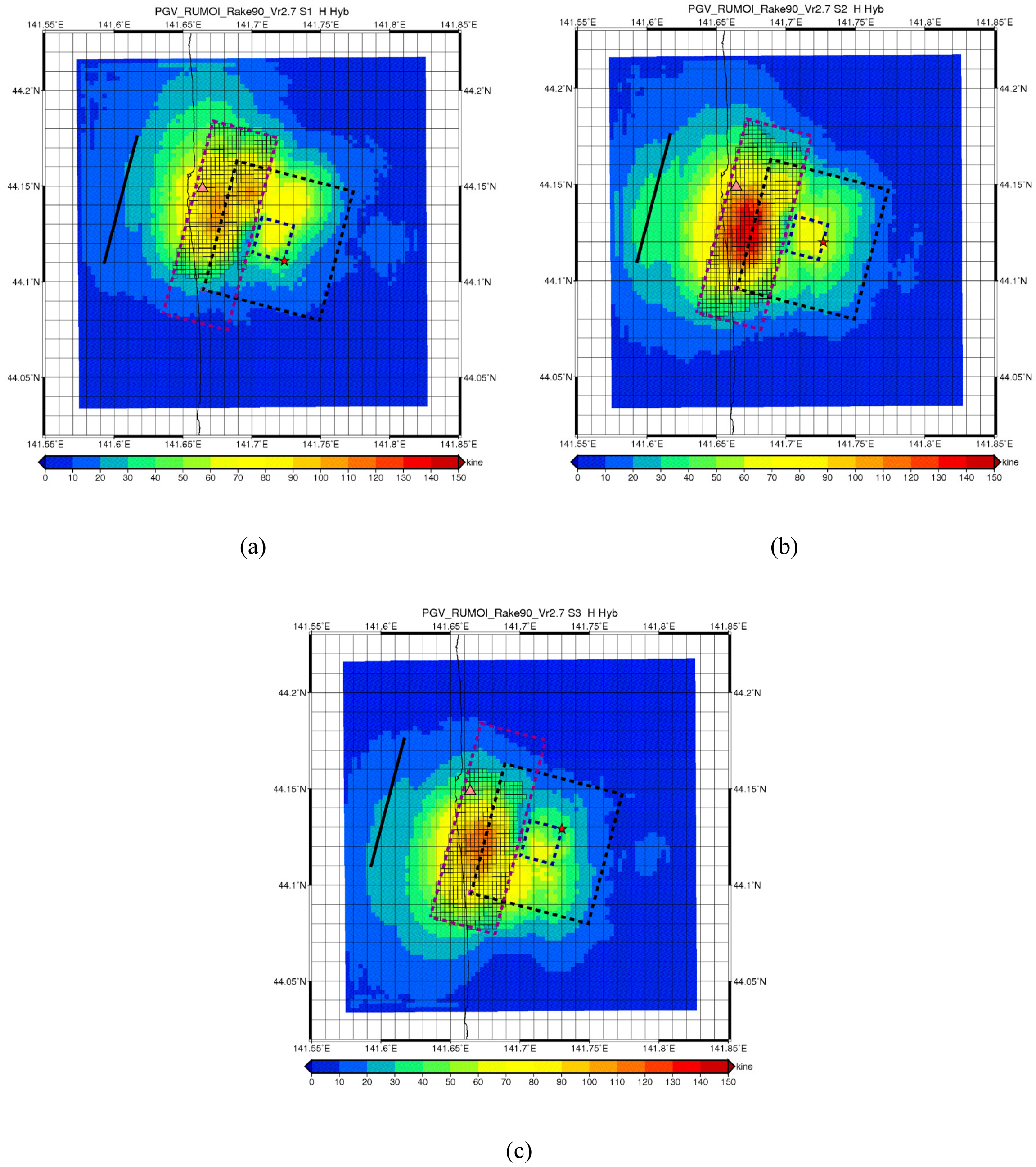

Figure 9. PGV distribution map for variation of rupture starting point. Star denotes the rupture starting point on the bottom edge of SMGA at (a) southern side, (b) middle side, and (c) northern side, respectively. Shaded zone shows the predominant area of NFRD effect using PGV attenuation curve.

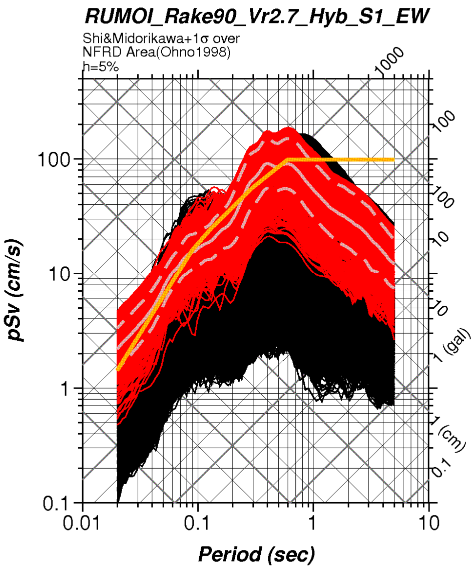

(a)

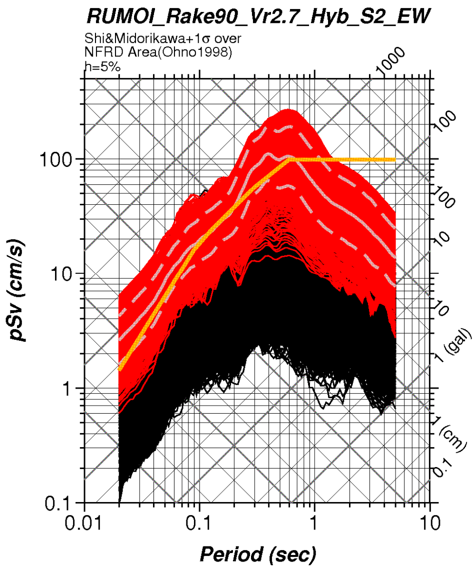

(b)

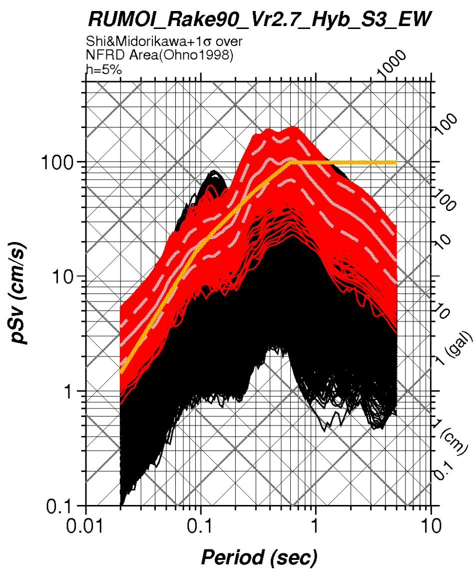

(c)

Figure 10. Examples of the pSv (red solid line) for EW components in shaded zone as shown in Fig. 9. Rupture starting point on the bottom edge of SMGA at (a) southern side, (b) middle side, and (c) northern side. White solid line denotes averaged pSv. White broken lines denote standard deviations.

5. CONCLUSIONS

We investigated the near-fault rupture directivity effect (NFRD effect) in strong ground motions during the 2004 Rumoi earthquake (*M*j 6.1). Strong ground motions over 1000 cm/s^2 and 70 cm/s were recorded at the nearest strong-motion station (HKD020). We calculated seismograms near the fault area (20 km x 20 km) and made a PGV distribution map using Hybrid simulation combining 3D-FDM and SGF methods. Strong ground motions over 70cm/s, which are affected by the NFRD effect, appeared near the fault area using the Hybrid simulation. We extracted the predominant area of the NFRD effect using the criteria of Ohno et al. (1998). Additionally we attempted to select a large PGV zone in the predominant area of the NFRD effect using a PGV attenuation curve (Si and Midorikawa, 1999). As a result, we successfully selected a large PGV zone affected by the NFRD effect near the fault area.

ACKNOWLEDGEMENT
We sincerely thank NIED (National Research Institute for Earth Science and Disaster Prevention) for providing the strong motion data (K-NET, KiK-net). The hypocenter information was provided by JMA and moment tensor by F-net of NIED. This study was supported by the Nuclear Safety Commission of Japan (NSC).

REFERENCES

Boore, D. M. (1983). Stochastic simulation of high-frequency ground motions based on seismological models of the radiation spectra, *Bull. Seism. Soc. Am.*, **73**, 1865-1894

Bouchon, M. (1981). A simple method to calculate Green's function for elastic layered media, *Bull. Seism. Soc. Am.*, **71**. 959-971.

Headquarters for Earthquake Research Promotion (2009). Ground motion assessment by fault rupture models (in Japanese), http://www.jishin.go.jp/main/chousa/09_yosokuchizu/g_furoku3.pdf.

Kagawa, T. (2004). Developing a stochastic Green's function method having more accuracy in long period range to be used in the Hybrid method, *Journal of JAEE*, **4**, **2**, 21-32. (in Japanese).

Kato, K., Miyakoshi, K., Takamura, M., Inoue, D., Ueta, K. and Dan, K. (2004). Earthquake ground motions by blind faults in the upper crust, Categorization of earthquakes based on geological survey and examination of the upper level from strong motion records, *Journal of JAEE*, **4**, **4**, 46-86. (in Japanese).

Kennett, B. L. N. and Kerry, N. J. (1979). Seismic waves in a stratified half space, *Geophys. J. R. astr. Soc.*, **57**. 557-583.

Maeda, T. and Sasatani, T. (2009). Strong ground motions from an Mj 6.1 inland crustal earthquake in Hokkaido, Japan: the 2004 Rumoi earthquake, *Earth Planets Space*, **61**, 689-701.

Miyakoshi, K., Maeda, T., Sasatani, T., Kamae, K. and Irikura, K. (2010). Mechanism of large ground motion at HKD020 during the 2004 Rumoi earthquake (Mj6.1), Hokkaido, Japan, Japan Geoscience Union Meeting 2010, SSS016-P22.

Ohno, S., Takemura, M. and Kobayashi, Y. (1998). Near-fault rupture directivity effect on strong ground motions, Proc. of the 10th Japan Earthquake Engineering Symposium, 133-138. (in Japanese).

Pitarka, A. (1999). 3D elastic finite-difference modeling of seismic motion using staggered-grid with non-uniform spacing, *Bull. Seism. Soc. Am.*, **89**, 54-68.

Si, H. and Midorikawa, S. (1999). New attenuation relationships for peak ground acceleration and velocity considering effects of fault type and site condition, *J. Struct. Constr. Eng.*, *AIJ*, **523**, 63-70. (in Japanese).

Somerville, P. G., Smith, N. F., Graves, R. W. and Abrahamson, N. A. (1997). Modification of empirical strong ground motion attenuation relations to include the amplitude and duration effects of rupture directivity, *Seism. Res. Lett.*, **68**, 199-222.